Centralized Rainfall Estimation using Carrier-to-Noise of Satellite Communication Links

Ahmad Gharanjik, *Member, IEEE,* Bhavani Shankar M. R., *Senior Member, IEEE,* Frank Zimmer, *Member, IEEE,* and Björn Ottersten, *Fellow, IEEE*

***Abstract*—In this work, we present a centralized method for real-time rainfall estimation using Carrier-to-Noise power ratio (C/N) measurements from broadband satellite communication networks. The C/N data of both forward-link and return-link are collected by the gateway station (GW) from the user terminals in the broadband satellite communication network and stored in a database. The C/N for such Ka-band scenarios is impaired mainly by the rainfall. Using signal processing and machine learning techniques, we develop an algorithm for real-time rainfall estimation. Extracting relevant features from C/N, we use artificial neural network in order to distinguish the rain events from dry events. We then determine the signal attenuation corresponding to the rain events and examine an empirical relationship between rainfall rate and signal attenuation. Experimental results are promising and prove the high potential of satellite communication links for real environment monitoring, particularly rainfall estimation.**

***Index Terms*—Satellite communication, rainfall estimation, microwave propagation, Ka-band, Broadband communication, Artificial neural networks**

I. Introduction

Rain has a significant influence on the global economy. It is of paramount importance to agriculture since it is the most effective means of watering. A regular rain pattern is usually vital to healthy crops; significant variations in rainfall can be harmful, even devastating them. Thus rainfall influences the success of harvest, creating inflationary/ deflationary effect on agricultural produce and societal consumption of the same. It creates river and flash floods, which may vanish homes and businesses causing loss of life and property. While river floods have been monitored, the changes in climate has led to significant increase in flash floods that can occur at any place. These have a clear impact on the insurance business since the sector is tasked with offering damage coverage in case these unfortunate events occur. Further, rainfall can interrupt traffic connections, supplies for electricity, gas, water and medical care bringing economic activity to a standstill [1], [2]. Given the critical impact of rain, it becomes essential to manage resources, operations and infrastructure taking rainfall into account; these include advice on tilling and harvesting, water management, infrastructure and transportation and steps for soil conservation. This task requires estimation of rainfall accurately over the given region of interest.

The measurement of rainfall might appear to be straightforward at first. However, rainfall has high spatio-temporal dynamics; it varies with location and time. This phenomenon makes it very difficult to measure rainfall satisfactorily. Therefore, denser measurement networks, that are always on, are required in order to capture this variability. Creating, operating and managing a dense measurement network entails high CAPEX (capital expense)/ OPEX (operating expense) cost; this is reflected in the current solutions for rainfall measurement discussed below:

1) Rain Gauge: The first known rainfall measurement dates back to the fourth century BC in India, where people used a bowl as a rain gauge and the readings were used for agricultural purpose [3]. Surprisingly, not much has changed since then from a measurement perspective. It continues to be the most common and accurate method for measuring the rainfall. However, it is not practical to install and maintain large number of closely spaced rain gauges to cover large areas due to high operational costs [4].
2) Weather Radar: This technique can measure area of radius up to 200 Km but suffers from low accuracy in rainfall measurement. In particular, the sensitive Weather radars (in C-band and beyond) are unable to detect the rain cell behind a convective rain cell. Another drawback of weather radar is its high cost: a new installation requires CAPEX of € 2.5 million and OPEX of € 76,000/year [5].
3) Infrared Satellite Imagery: An overview of precipitation measurements from Space is presented in [6]. This method could provide global coverage but its accuracy is known to be very limited and has a large discrepancy with actual rain gauge measurements [7]. For instance, *STAR Satellite Rainfall Estimates* (Hydro−Estimator) uses infrared data from NOAA's Geostationary Operational Environmental Satellites (GOES) to estimate rainfall rates [8]. Further, the CAPEX and OPEX for such a system are rather high.
4) Microwave Links in Mobile Networks: Although possibility of rainfall monitoring using microwave (MW) links is theoretically well established [4], [9]–[11], it has not been commercially deployed in real world due to unavailability of enough microwave links for data collection. In 2006, Messer et al. proposed the use of commercial MW links in mobile networks for rainfall monitoring [12]. Thereafter, many investigations have been conducted using commercial MW links [13]–[17]. Experimental results confirmed the accuracy of this approach and proved its potential for commercialization. However, an issue with this approach is the sparse network of MW links in rural and remote areas where,

unfortunately, limited rainfall data is available. Further, additional effort is needed for data procurement since MW links are operated by different entities at different regions.

In addition to these commercially deployed mechanisms, there are a few other proposals for rainfall estimation which rely on satellite data, [18]–[23]. In [18]–[20], authors have investigated rainfall estimations using Ku-band links of broadcast television (TV) satellites. The received signal power level is collected form the satellite TV receiver at user side. In [21] and [22], authors have considered a similar scenario but using Ka-band broadband satellite communication links. The experimental results confirmed feasibility of these approaches for rainfall estimation with acceptable accuracy. The ITU-R model, typically used in such papers, has been shown to underestimate the rain attenuation in tropics and specific attenuation coefficients had been derived using measurements values in [24]–[26]. Impact of rainfall on the satellite communication links is a well investigated field of research [27]–[33].

However, these schemes can only collect data from single UT and cannot scale-up which makes these approaches less suitable for real-world scenarios and commercialization attempts where rainfall data for wider coverage area is needed. In [23], a hypothesis of 3D rainfall tomography using LEO satellite was introduced which, however, is far from being deployed in real-world currently.

Motivated by these challenges, in this paper we propose a real-time and centralized rainfall estimation approach using C/N data fed back from the user terminal (UT) to the satellite gateway (GW) in a broadband interactive satellite system. The collected C/N data is then processed building on empirical model relating the rainfall rate to signal attenuation and machine learning techniques to obtain rainfall estimates. This approach can be seen as complementary solution to rainfall estimation method using terrestrial MW links and overcomes its drawbacks. In addition to the presenting the methodology, the paper also validates the proposed approach using field measurement from the satellite operator SES and on-site rain-gauges.

The key advantages of the proposed method are:

1) *Wider Coverage:* Satellite UTs are usually distributed in rural and remote area, therefore the use of satellite MW links enable the prospect of collecting rainfall data from these areas. This provides for a dense sampling of the coverage area. The proposed approach has the potential to exploit $300,000$ UTs (and growing) across Europe and more that 2 million UTs around the world. The dense sampling enhances the spatial accuracy of estimates.
2) *Centralized Estimation:* Since the C/N is sourced from the GW and not from the UTs directly, there is already an aggregation of large amount of data at each GW. This allows for a centralized estimation of rainfall over a wide coverage. Further, there are a few satellite operators and Internet service providers (ISPs) who further aggregate data from multiple GWs; this allows for easy procurement of data unlike in the case of MW links.

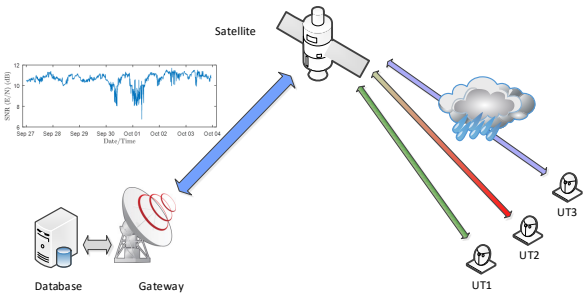

Fig. 1. Architecture of a Broadband Satellite Communication Systems. The C/N data of the FWD and RTN links are collected by the gateway and stored at a database. We use these data for rainfall estimation.

3) *Real Time Data:* The average C/N is fed back to the GW every 5 minutes, with the possibility to achieve higher temporal resolution with minor modifications to the system. This coupled with the ease of procuring aggregated data allows for real time estimation of rainfall.
4) *Cost:* The proposed method exploits available infrastructure and hence offers a low-cost alternative.

Beside considering above advantages, it deserves consideration that measurements from UT can be available only if terminals are switched on and a link has been established. It should be noted that a high level of link availabilities are guaranteed through service agreements. The impact of non-operational or failed devices is lower than rain-gauges due to the high sampling of the coverage area.

The paper is organized as follows: Section II describes the broadband satellite communication set-up used in the paper for collecting the C/N and validates the principle behind the approach. Section III explains the approach for classifying rain and dry events as well as estimating the baseline signal in the case of rain event. In Section IV, two models for mapping the signal attenuation to rainfall rate are investigated. Finally, Section V presents the performance of the rainfall estimation algorithm and compares it with existing approaches in the literature.

II. Rainfall Estimation using Broadband Satellite Communication System

A. Scenario

Broadband satellite systems offer bidirectional communications between the GW stations and UTs enabling interactive satellite services (such as internet provisioning), see Fig. 1. The link from the GW to UTs is called the forward (FWD) link and the link from UTs to the GW is the return (RTN) link. In a typical broadband satellite system, content to/from remote UTs are aggregated at the GW stations; such stations are operated and maintained typically by satellite operators. We further assume that the UTs do not experience interference from each others' transmissions; this is feasible, e.g., if they are provisioned on different resources (time, frequency).

To maintain a certain level of quality of service for users, GW stations continuously monitor the FWD and RTN links

(enabled by the bidirectional link). The C/N parameter measures quality of the communication link and received signals. For the FWD link, the UTs estimate this parameter and send it back to the GW station using the standard air-interface protocol. Additionally, the GW also measures the C/N using the transmissions from the RTN link. Thus the GW has access to end-to-end C/N on both the links. Further, it is generally assumed that the link between GW and the satellite (feeder link) is ideal. This is due to the fact that the transmit/receive antenna gain of the GW is very high. Moreover, in the case of heavy fading at the feeder link, site diversity is used for fade mitigation. Therefore, the end-to-end C/N of FWD and RTN links is dominated by the C/N of the user link (links between satellite and UTs). As a result, it can be assumed that variations of the end-to-end C/N are mainly caused by the user links.

B. Rainfall Estimation Concept

In the considered scenario where UTs do not interference, the C/N parameter is highly dependent on the link conditions and is mainly affected by the rain attenuation at the operational Ka-band frequencies (broadband satellite) [34]. Therefore, there is a clear correlation between the C/N variations and amount of the rainfall. Towards this, we first present an experimental set-up to illustrate the correlation. Subsequently, this correlation will be exploited in the proposed approach to estimate the amount of rainfall.

In order to illustrate our proposed method, we have exploited the experimental system installed at SES Techcom in Betzdorf, Luxembourg. The system includes a broadband satellite UT and a weather station equipped with rain gauge. The UT receives broadband services from ASTRA 2F satellite located at the orbital position of 28.2 E. The links from satellite to UT operate at K-Band ($19.70 - 20.20$ GHz) while the links from UT to satellite is at Ka-Band ($29.40 - 30.00$ GHz). The Elevation and Azimuth angles of the links are $29.4°$ and $151.8°$, respectively.

Average C/N for both FWD and RTN links are available at the GW station every five minutes. These measurements, in fact, correspond to C/Naveraged over the 5 minute duration and stored in a database. Simultaneously, a co-located weather station reports the average rain intensity (mm/h) every minute. In order to have consistent temporal resolution, we aggregate the rain intensity data and transform them to a five minute average rain intensity represented by $r(n)$.

We use weather station data for labeling the C/N measurements with dry or rain label. It is important to note that C/N signals represent a path-averaged process impacted by the rainfall over the satellite slant path while weather station corresponds to an in-situ point process. Therefore, it is possible that some C/N measurements are labeled incorrectly which will lead to some errors in the classification. Theoretical explanation of mislabeling impact on classification is a huge topic in itself and is outside of the scope of this paper. Interested readers can refer to following survey paper [35]. In subsequent sections, we present the features for classification and elaborate on the classification errors in Section V. For the

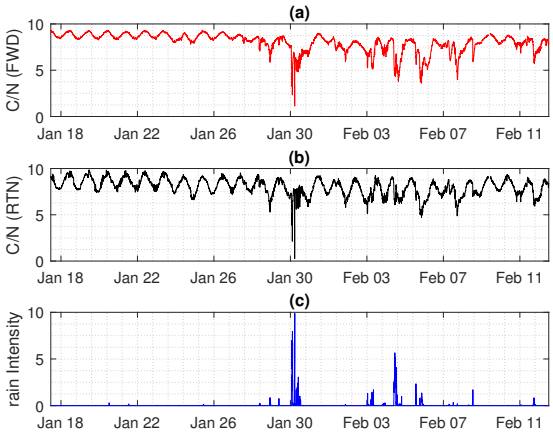

Fig. 2. Sample data from the dataset: (a) FWD link C/N in dB, (b) RTN link C/N in dB and (c) rain intensity in mm/h, $r(n)$. Location, Betzdorf, Luxembourg.

experiment, we have collected C/N and rain intensity data for almost 3 months: from November 2016 to February 2017 for training the rainfall estimation algorithm and data of June 2017 for testing it. This corresponds to about $K = 27500$ labeled training data points and 8200 labeled test data points. Fig. 2 shows a sample data from the training dataset. It can clearly be observed that during the rain event, C/N parameter drops indicating the correlation.

III. Baseline (Reference Level) Estimation

A. Components of C/N

The first step towards estimating the rainfall from C/N measurements is to determine the amount of signal attenuation caused by rainfall during the rain event. Central to this, is an understanding of the various components constituting the C/N and the impact of rainfall on them. To this end, let us denote C/N for FWD and RTN links by $C_F(n)$ and $C_R(n)$, respectively, where n is the index of measurement (data sample). It should be noted that data indexing starts from midnight and has a resolution of 5 minutes, i.e. $n = 2$ represents $00:05$ AM of the first day of data collection.

Radio-wave propagation (and C/N) on Earth-Space links in millimeter wave frequencies is impacted by different tropospheric effects [29], [31] including (i) Gaseous absorption due to oxygen and water vapour, (ii) cloud attenuation, (iii) rain attenuation and (iv) scintillations. Of the four effects above, the one with considerable variation is rain attenuation. It is worth mentioning that C/N is affected by interference terms like co-channel interference. Such perturbations have high spatio-temporal dynamics and can affect the sensitivity of C/N to rain attenuation. However, recalling from I. interference in the considered scenario is limited and the same is reflected in the measurement set-up. Fig. 2 confirms the impact of rain attenuation on the C/N variations.

It can also be seen from Fig. 2 that C/N has a low frequency component that varies slowly over the time even during clear sky. This is due to the fact that the satellite is not in a perfectly

geostationary orbit; its orbit is slightly inclined with respect to equatorial plane and has quasi-circular (elliptic) orbit. The cycle duration of this component is 24 hours or 288 C/N samples.

Therefore, we can decompose the C/N (in dB) as,

$$C_z(n) = B_z(n) - A_z(n) + s_z(n), \tag{1}$$

where $z \in \{F, R\}$ denotes the choice of FWD or RTN links. Here, $s_z(n)$ characterizes the impact of quasi-circular orbit, $B_z(n)$ is the baseline (reference level) that corresponds to the expected C/N in dry (no-rain) situation assuming a fixed UT position (excluding $s_z(n)$). It should be noted that $B_z(n)$ also includes impact of Gaseous absorption, cloud attenuation, scintillations and noise in the MW link. $A_z(n)$ shows the impact of rain attenuation; naturally, this is zero in dry situations.

1) Impact of Elliptic Orbit: The component, $s_z(n)$ is deterministic since the satellite orbit is predetermined. Using Discrete Fourier Transformation (DFT), we can find this component for FWD and RTN links respectively as,

$$s_F(n) = 0.81 \sin(2\pi(\hat{n} - 46)/T_0), \tag{2}$$
$$s_R(n) = 0.39 \sin(2\pi(\hat{n} - 46)/T_0), \tag{3}$$

where $T_0 = 288$ is the number of $C_z(n)$ samples in one cycle duration (24 hours) and $\hat{n} \equiv n \pmod{288}$ (index of data sample with respect to just concluded midnight). Fig. 3 depicts $s_F(n)$ and $s_R(n)$ along with corresponding $C_z(n)$ from which its mean value, m_z, is deducted for better illustration. It can be seen that $s_F(n)$ and $s_R(n)$ capture the main variation of the C/N due to inclined orbit.

2) Baseline C/N in dry case: Since the components $s_F(n), s_R(n)$ are independent of the tropospheric effects, we can remove them from the C/N measurements in order to have a better estimation of the variations caused solely by rainfall. Therefore, we define $\bar{C}_z(n)$ as,

$$\bar{C}_z(n) = C_z(n) - s_z(n) = B_z(n) - A_z(n). \tag{4}$$

It is worth mentioning that $\bar{C}_z(n)$ is a known signal but $B_z(n)$ and $A_z(n)$ need to be estimated. We observe that baseline can be estimated as $B_z(n) = \bar{C}_z(n)$ during dry events since, $A_z(n) = 0$. However, it is challenging to determine the baseline during rain event. One possible way is to estimate it from baseline obtained from the closest observed dry event. Particularly, we can have,

$$B_z(n) = \begin{cases} \bar{C}_z(n) & \text{for dry period} \\ \bar{C}_z(n_d) & \text{for rain period} \end{cases} \tag{5}$$

where $\bar{C}_z(n_d)$ represents the closest observed dry event. Therefore, in order to calculate the baseline we first need to distinguish the rain event from dry events. In the sequel, we introduce an algorithm that can classify the event in real-time.

B. Rain-Dry Event Classification Algorithm

In this section, we detail the proposed classification algorithm which is based on Artificial Neural Network (ANN).

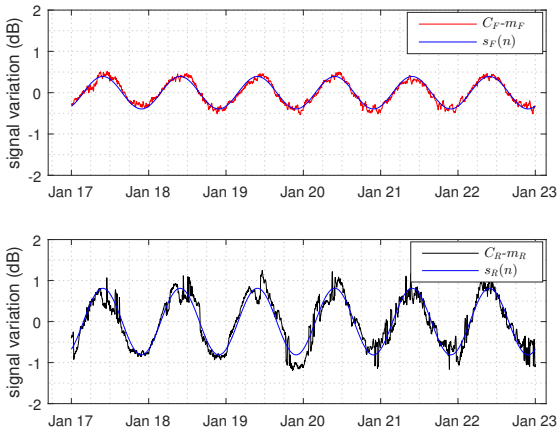

Fig. 3. Variation of C/N due to inclined GEO orbit in clear sky condition where m_z is the mean of C_z over the entire duration.

The first step towards efficient classification is to define a set of features that capture the distinguishing aspects between different events.

1) Feature Extraction: The features considered in this work along with the motivation for their choice are mentioned below:

1) Feature 1: Local Standard Deviation: It can be observed from Fig. 2 that during the rain event, variation of the C/N signal is high and scale of variations depends on intensity of the rain. Hence, local variation of the C/N signal can be a useful feature for identifying rain/dry events. These variations can be encapsulated by the local standard deviation [20], [36] which is defined as follows,

$$S^z_{W_n}(n) = \left[\frac{1}{N_W} \sum_{k \in W_n} \left(\bar{C}_z(k) - m_{W_n} \right)^2 \right]^{\frac{1}{2}}, \tag{6}$$

where $W_n = [n - N_W + 1, n]$ is the moving time window with N_W observation samples. Also m_{W_n} is the local average of $\bar{C}_z(n)$ and defined as,

$$m_{W_n} = \frac{1}{N_W} \sum_{k \in W_n} \bar{C}_z(k). \tag{7}$$

2) Feature 2: Deviation from Mean: Besides high variation of C/N signal during rain events, it is expected that its value drops considerably with respect to long-term average C/N. This characteristic can be represented by d_z, defined as follows,

$$d_z(n) = C_z(n) - m_z(n), \tag{8}$$

where $m_z(n)$ is the long-term average of $C_z(n)$ and defined as,

$$m_z(n) = \frac{1}{n} \sum_{i=1}^{n} C_z(i). \tag{9}$$

Based on the aforementioned choice and the availability of C/N measurements for both RTN and FWD links, we can

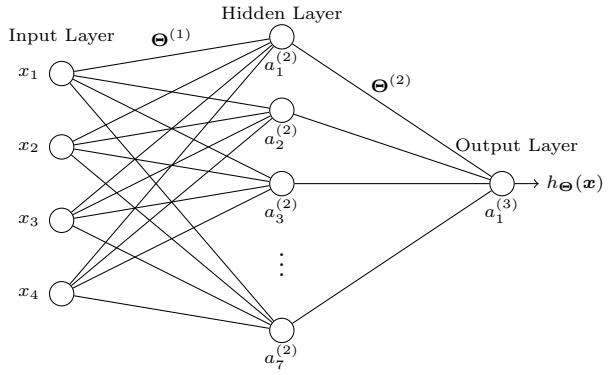

Fig. 4. Feed-Forward Artificial Neural Network for rain/dry classification

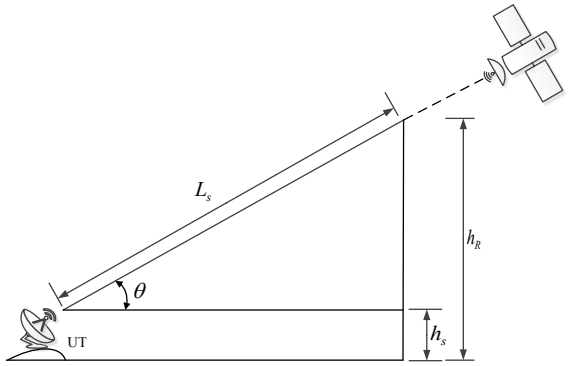

Fig. 5. Geometry of the satellite slant path

define a $K \times 4$ matrix $\boldsymbol{X}$ whose rows are the feature vectors as follows,

$$\boldsymbol{X}(n,:) = \left[S^F_{W_n}(n), S^R_{W_n}(n), d_F(n), d_R(n)\right]. \tag{10}$$

These features are chosen in order to facilitate the differentiation of rain and dry events. Recalling that $r(n)$ denotes the rain intensity, we define the labels (rain or dry) for each data sample as follows,

$$y(n) = \begin{cases} 1 & \text{if } r(n) > 0 \\ 0 & \text{if } r(n) = 0 \end{cases}. \tag{11}$$

For the training set, we label the data based on rain intensity measured by the rain-gauge in the vicinity of the UT. We also define the label vector $\boldsymbol{y} = [y(1), y(2), \cdots, y(K)]^T$. The input and output dataset $(\boldsymbol{X}, \boldsymbol{y})$ can then be used for training the ANN classification algorithm to perform classification in test scenarios.

2) Artificial Neural Network: We have deployed artificial neural network for solving the resulting classification problem since it outperforms other techniques like SVM (Support Vector Machine) as size of the training dataset increases. Specifically, we have considered a feed-forward neural network [37] comprising three layers as depicted by Fig. 4.

Dimension of the input layer is 4, equal to the dimension of the feature vector. The hidden layer consists of 7 units, a value obtained by the general practice of having the number of hidden units to be less than twice the size of the input layer [38]. $\boldsymbol{\Theta}^{(j)}$ is the matrix of weights which shows the mapping from layer j to layer $j+1$ where input, hidden and output layers are labeled as 1, 2 and 3 respectively. Further, $a_i^{(j)}(n)$ is the activation of the unit i in layer j for input sample n. Let us define n^{th} input vector $\boldsymbol{x}(n) = [x_0(n), x_1(n), \cdots, x_4(n)]^T$ and $\boldsymbol{a}^{(j)}(n) = [a_0^{(j)}(n), a_1^{(j)}(n), \cdots, a_7^{(j)}(n)]^T$ where x_0 and $a_0^{(j)}$ are the bias units not shown in Fig. 4. Note that $\boldsymbol{a}^{(1)}(n) = \boldsymbol{x}(n)$. Note that for ease of reading we drop the sample index n. For the considered network we have following relation,

$$\boldsymbol{a}^{(j+1)} = g\left(\boldsymbol{\Theta}^{(j)}\boldsymbol{a}^{(j)}\right), \tag{12}$$

where $g(\cdot)$ is the element-wise sigmoid (logistic) activation function defined as,

$$g(z) = \frac{1}{1+e^{-z}}. \tag{13}$$

The output of the ANN can be written as $h_{\boldsymbol{\Theta}}(\boldsymbol{x}) = g\left(a_1^{(3)}\right)$ that estimates the posterior probabilities of rain event. In order to find the network weights, $\boldsymbol{\Theta}^{(1)}$ and $\boldsymbol{\Theta}^{(2)}$, we train the algorithm using `nprtool` from Neural Network toolbox of MATLAB [39]. Having the network weights, we can readily find the posterior probability of rain for any input vector $\boldsymbol{x}$ by $h_{\boldsymbol{\Theta}}(\boldsymbol{x})$. Then Rain-Dry classification rule is simple: we declare an input vector $\boldsymbol{x}$ corresponds to a

- Rain event if $h_{\boldsymbol{\Theta}}(\boldsymbol{x}) \geq p_{\text{T}}$
- Dry event if $h_{\boldsymbol{\Theta}}(\boldsymbol{x}) < p_{\text{T}}$.

Here p_T is a predefined threshold which is determined considering requisite operating point. Recall that the output of the ANN is 1 if the event is classified as rain and 0 otherwise.

Now that we can discriminate between rain and dry events, signal attenuation can be estimated using (4) and (5) as,

$$A_z(n) = \begin{cases} 0 & \text{for dry period} \\ \bar{C}_z(n_d) - \bar{C}_z(n) & \text{for rain period} \end{cases} \tag{14}$$

Note that for rainfall estimation we will use signal attenuation at FWD link, $A_F(n)$, since it provided better result than $A_R(n)$. From now on we denote $A_F(n)$ by A for simplicity.

IV. Rainfall Estimation

In this section, we will investigate two approaches for mapping the signal attenuation into rainfall rate. First we will study the model recommended by ITU, then will consider the model obtained by curve fitting using observed data.

A. ITU-R Model

The relation between rainfall rate and attenuation of MW signals is well established. The well-known model is proposed by Olsen et al. [11] which was adopted by ITU in its recommendations, [40], [41]. According to this model, specific

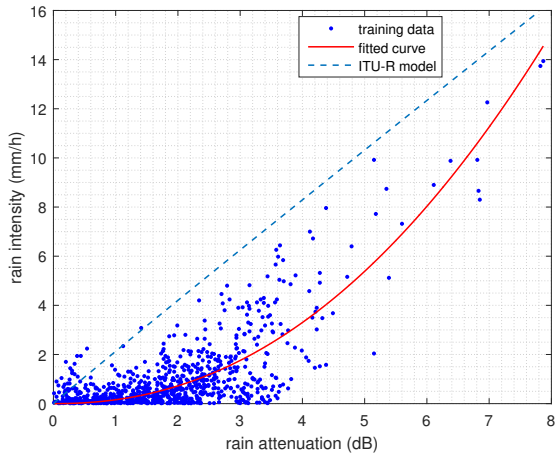

Fig. 6. Curve fitting using training data in order to find a empirical relation between rainfall rate and signal attenuation. ITU-R model is also shown.

attenuation γ (dB/Km) and rainfall rate (mm/h) have a power-law relationship,

$$\gamma = kR^{\alpha}. \tag{15}$$

The coefficients k and α depend on the frequency and polarization of the link. For the considered experimental setup at FWD link, these values can be calculated following ITU-R P.838-3 [40] as follows: $k = 0.0939$ and $\alpha = 1.0199$. The specific attenuation is defined as $\gamma = A/L_s$ where A is the signal attenuation at FWD link defined in (14). Here L_s (in Km) is the slant path length of satellite FWD link which is depicted in Fig. 5 and can be calculated as,

$$L_s = (h_R - h_s)/\sin\theta, \tag{16}$$

where h_s is height of the UT above the mean sea level, ($h_s = 0.28$ km for Betzdorf). It should be noted here, for simplicity, a homogeneous rainfall rate along a slant path up to the average rain height advocated by ITU-R P.839-4 [42] is assumed. The mean annual rain height above mean sea level, h_R, can be calculated using ITU-R P.839-4 [42] as,

$$h_R = h_0 + 0.36\,. \tag{17}$$

For the region of interest, Betzdorf, the value of h_0 can be calculate from ITU-R P.839-4 [42] that leads to $h_0 = 2.339$ km or equivalently $h_R = 2.699$ km. Using (16), we finally have $L_s = 4.9276$ km. The relation between rainfall rate and signal attenuation can be rewritten as,

$$R = 2.1295\, A^{0.9805}. \tag{18}$$

B. Curve Fitting

It can be seen from (18) and Fig. 6 that the expression obtained using ITU-R recommendation indicates a nearly linear relation between rainfall rate R and signal attenuation A.

Remark: We can notice from Fig. 6 that ITU-R model is not appropriate for the considered training dataset. One reason might be that in our dataset signal attenuation is a path averaged measurements but rainfall rate data represents a point process. However, in ITU-R model, both rainfall rate and signal attenuation correspond to path averaged measurements. Further understanding of the non-applicability of ITU-R model for considered data set is left for future investigation.

In view of this, we examined an empirical relationship between signal attenuation and rainfall rate assuming the latter to be homogeneous. In Fig. 6, the measurements are denoted with blue points for the training dataset. Considering the power-law relationship in (15), we can find the model that fits best the data in terms of least square error. By taking natural logarithm of both side of (15), it turns into a linear regression problem which can be solved readily. The derived expression can written as,

$$R = 0.1583\, A^{2.192}, \tag{19}$$

which is depicted by a red line in Fig. 6. Note that this expression corresponds to the region of interest, Betzdorf. For any other given location, the slant path length would be different which could be calculated using (16). Let us define slant path length corresponding to new location by $L_s' = \beta L_s$. Therefore, rainfall rate at any given location can be calculated by,

$$R = 0.1583\, (A/\beta)^{2.192}. \tag{20}$$

Henceforth, we use this expression in order to map the signal attenuation to rainfall rate.

V. Performance Evaluation and Discussion

In this section, we evaluate the performance of the proposed rainfall estimation approach. We used data from 17$^{\text{th}}$ of November 2016 to 20$^{\text{th}}$ of February 2017 for training the rain-dry classification algorithm and constructing a mapping model based on curve-fitting. We then used data from 1$^{\text{st}}$ of June to 29$^{\text{th}}$ of June, as test data to evaluate our approach. All the data were collected from the set-up mentioned in Section II-B. We first evaluate the proposed classification algorithm and then discuss the possible sources of error in rainfall estimation.

Fig. 7 presents the ROC (receiver operating characteristic) curve for the classification algorithm on the test dataset. It delineates two types of error as we change the threshold p_T defined in Section III-B2. The *false positive rate* is fraction of dry measurements that are falsely classified as a rain event. The *true positive rate* is fraction of rain events that correctly detected as rain event. Two types of error are linked to ROC curve as follows:

- *Type I Error*: false rainfall alarm = false positive rate
- *Type II Error*: missed rain = 1− true positive rate

ROC curve enables an understanding of the error performance of classification algorithm at different operating points. Each point on this curve corresponds to a given value of p_T. For instance when $p_T = 0.18$, the Type I error is 6% and Type II error will be 9.5%. By changing the value of p_T and calculating the Type I and Type II errors, we could have the ROC curve. Considering this operating point, we can confirm that our proposed classification algorithm has comparable performance to those investigated in [36] and [43]. More

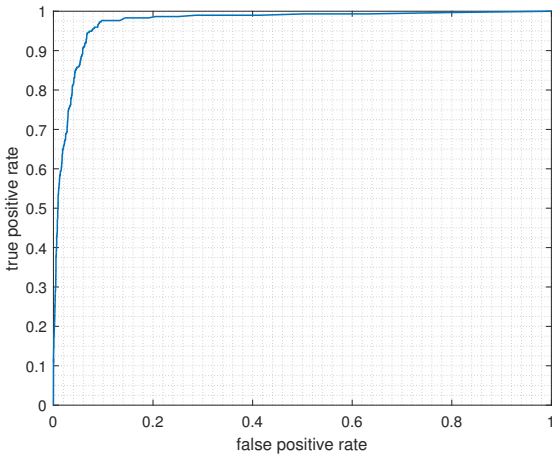

Fig. 7. ROC curve for the classification algorithm on the test dataset.

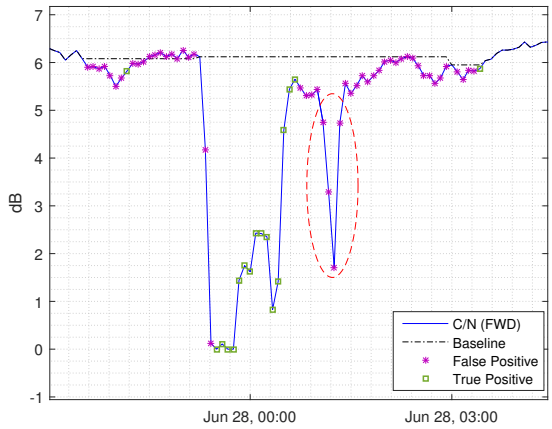

Fig. 9. C/N(FWD) signal along with estimated baseline signal and output of classification algorithm for specific event shown in Fig. 8.

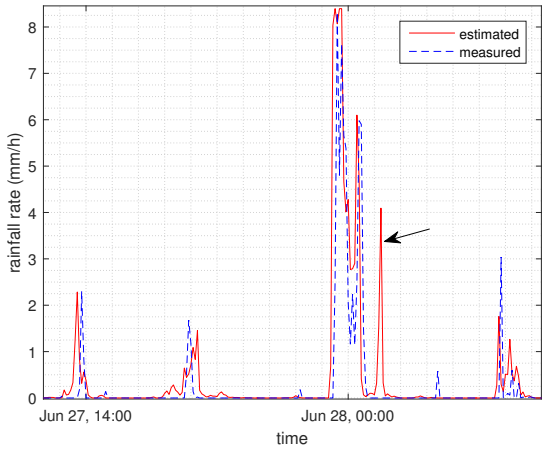

Fig. 8. Five minutes' average rainfall rate : Comparison between rain gauge readings and values estimated by our proposed algorithm.

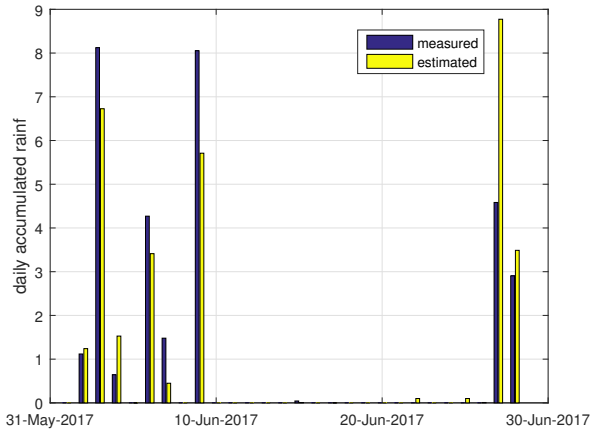

Fig. 10. Comparison between estimated and measured daily accumulated rain for test dataset

specifically, terrestrial microwave links were used in [43] for dry and rain events classification and resulted in Type I error of 6% and Type II error of 14.4%.

Fig. 8 shows the five minutes' average rainfall rain comparison between rain gauge at Betzdorf and estimated by proposed algorithm. The blue dashed line shows the measured values by the rain gauge and solid red line present the estimated rainfall rate. The figure shows a good agreement between two time series. It can also be observed that there is a time lag between estimated and measured rainfall rate. This can be justified by cloud movement and the fact that rain clouds could impact the satellite slant path ($L_s \approx 5$ Km) before reaching to the location of rain gauge at Betzdorf. Moreover, drop falling velocity can also contribute to this time lag.

It can also be observed in Fig. 8 that a rain event declared by the proposed algorithm (pointed by black arrow) but was not reported by rain gauge measurements. This again could be due to estimating point measurements (rain gauge values) by path-averaged measurements on the satellite link. More specifically, when there are scatter showers along the slant path, it will be detected by our proposed approach but might not be reported by the rain gauge. Fig. 9 reveals more details about the performance of proposed algorithm regarding the specific event pointed in Fig. 8.

The C/N(FWD) along with estimated baseline signal and output of classification algorithm are displayed in Fig. 9. The red dashed oval denotes the event which was declared as rain but reported as dry by rain gauge. Therefore, corresponding data samples were shown as false positive. However, considering the large signal drop, we can support that proposed algorithm detected the rain event correctly. This sort of error contributes to Type I error and can be reduced by better labeling of the data through employing multiple rain gauges along the projected slant path.

We can also notice from Fig. 9 that there are some false positive samples where C/N is very close to the estimated baseline, resulting in small signal attenuation, refer to (4). Subsequently, estimated rainfall rate will be negligible for those samples. Then, even though those samples classified incorrectly by proposed classification algorithm, very small

estimated rainfall rate can be used to restore the classification false positive error.

It is worth mentioning that we assumed that baseline signal is fixed during the rain event, please refer to (5), as shown in Fig. 9. However, baseline will change during the rain event mainly due to wet antenna attenuation (WAA) [44]. Considering WAA impact will improve the accuracy of the algorithm.

Finally, Fig. 10 shows the estimated and measured daily accumulated rainfall. It can be seen that all rainy days were detected accurately by the proposed algorithm and there is a relative agreement between estimated and measured values. However, there is still room for improving the performance of algorithm by better labeling (path-averaged vs. point process issues) and considering WAA.

VI. Conclusion

We introduced and investigated a centralized and real-time method for rainfall estimation. This approach is based on opportunistic use of C/N measurements from broadband satellite communication networks. The proposed algorithm has two main parts: first, it classifies the events, using an artificial neural network, into rain or dry which is used for estimating the baseline C/N value. The measurements classified as rain-events are subsequently processed using a curve fitting algorithm to obtain rainfall rate. Performance of the proposed algorithm is comparable to approaches that use terrestrial MW links for rainfall estimation. Possible sources of errors, namely wet antenna attenuation and inaccurate labeling of path-averaged data, are listed, whose mitigation can further improve the performance of the proposed method. Incorporation of non-homogeneous rain rate, dynamic rain height and Drop Size Distribution are some of the future research directions for possible improvement. The idea opens up a novel avenue for the use of satellite data for environmental monitoring as well as an interesting research field on combining machine learning with model based processing.

Acknowledgment

This work was partially funded by the Luxembourg National Research Fund (FNR) for the Proof of Concept project RAFAEL bearing contract POC/17/ 11648950.

The authors would like to thank Ralf Kierspel and Thorsten Rau from SES Techcom for their help in data acquisition process, Dr. Andrew Ferrone from Ministry of Agriculture, Viticulture and Consumer Protection, Luxembourg and Dr. Kumar Vijay Mishra, University of Iowa, for interesting discussions.

References

[1] C. Kidd, A. Becker, G. J. Huffman, C. L. Muller, P. Joe, G. Skofronick-Jackson, and D. B. Kirschbaum, "So, how much of the earths surface is covered by rain gauges?" *Bulletin of the American Meteorological Society*, vol. 98, no. 1, pp. 69–78, 2017.

[2] H. Messer, A. Zinevich, and P. Alpert, "Environmental sensor networks using existing wireless communication systems for rainfall and wind velocity measurements," *IEEE Instrumentation & Measurement Magazine*, vol. 15, no. 2, 2012.

[3] I. Strangeways, "A history of rain gauges," *Weather*, vol. 65, no. 5, pp. 133–138, 2010.

[4] A. Rahimi, A. Holt, G. Upton, and R. Cummings, "Use of dual-frequency microwave links for measuring path-averaged rainfall," *Journal of Geophysical Research: Atmospheres*, vol. 108, no. D15, 2003.

[5] "Ericsson mobility report," June 2016. [Online]. Available: https://www.ericsson.com/res/docs/2016/ericsson-mobility-report-2016.pdf

[6] V. Levizzani, "Precipitation measurements from space," in *2006 First European Conference on Antennas and Propagation*, Nov 2006, pp. 1–5.

[7] B. Geerts. Satellite-based rainfall estimation. [Online]. Available: http://www-das.uwyo.edu/~geerts/cwx/notes/chap10/satellite_rain.html

[8] NOAA, "Star satellite rainfall estimates." [Online]. Available: https://www.star.nesdis.noaa.gov/smcd/emb/ff/index.php

[9] R. A. Semplak and R. Turrin, "Some measurements of attenuation by rainfall at 18.5 ghz," *Bell Labs Technical Journal*, vol. 48, no. 6, pp. 1767–1787, 1969.

[10] R. Crane, "Propagation phenomena affecting satellite communication systems operating in the centimeter and millimeter wavelength bands," *Proceedings of the IEEE*, vol. 59, no. 2, pp. 173–188, 1971.

[11] R. Olsen, D. V. Rogers, and D. Hodge, "The ar b relation in the calculation of rain attenuation," *IEEE Transactions on Antennas and Propagation*, vol. 26, no. 2, pp. 318–329, 1978.

[12] H. Messer, A. Zinevich, and P. Alpert, "Environmental monitoring by wireless communication networks," *Science*, vol. 312, no. 5774, pp. 713–713, 2006.

[13] A. Zinevich, P. Alpert, and H. Messer, "Estimation of rainfall fields using commercial microwave communication networks of variable density," *Advances in water resources*, vol. 31, no. 11, pp. 1470–1480, 2008.

[14] H. Leijnse, R. Uijlenhoet, and J. Stricker, "Rainfall measurement using radio links from cellular communication networks," *Water Resources Research*, vol. 43, no. 3, 2007.

[15] O. Goldshtein, H. Messer, and A. Zinevich, "Rain rate estimation using measurements from commercial telecommunications links," *IEEE Transactions on Signal Processing*, vol. 57, no. 4, pp. 1616–1625, 2009.

[16] A. Overeem, H. Leijnse, and R. Uijlenhoet, "Country-wide rainfall maps from cellular communication networks," *Proceedings of the National Academy of Sciences*, vol. 110, no. 8, pp. 2741–2745, 2013.

[17] P. Alpert, H. Messer, and N. David, "Meteorology: Mobile networks aid weather monitoring," *Nature*, vol. 537, no. 7622, pp. 617–617, 2016.

[18] C. H. Arslan, K. Aydin, J. Urbina, and L. P. Dyrud, "Rainfall measurements using satellite downlink attenuation," in *2014 IEEE Geoscience and Remote Sensing Symposium*, July 2014, pp. 4111–4114.

[19] F. Mercier, L. Barthès, and C. Mallet, "Estimation of finescale rainfall fields using broadcast TV satellite links and a 4DVAR assimilation method," *Journal of Atmospheric and Oceanic Technology*, vol. 32, no. 10, pp. 1709–1728, 2015.

[20] L. Barthès and C. Mallet, "Rainfall measurement from opportunistic use of earth-space link in ku band," *Atmospheric Measurement Techniques*, vol. 6, no. 8, pp. 2181–2193, 2013.

[21] C. Mugnai, F. Cuccoli, and F. Sermi, "Rainfall estimation with a commercial tool for satellite internet in Ka band: concept and preliminary data analysis," in *SPIE Remote Sensing*. International Society for Optics and Photonics, 2014, pp. 923 904–923 904.

[22] C. Mugnai, F. Sermi, F. Cuccoli, and L. Facheris, "Rainfall estimation with a commercial tool for satellite internet in Ka band: Model evolution and results," in *2015 IEEE International Geoscience and Remote Sensing Symposium (IGARSS)*, July 2015, pp. 890–893.

[23] H. Defeng, X. Lu, F. Xuxiang, and W. Wanyu, "A hypothesis of 3d rainfall tomography using satellite signals," *Journal of Communications and Information Networks*, vol. 1, no. 1, pp. 134–142, 2016.

[24] A. F. Ismail, K. Badron, A. A. H. Yaccop, and Y. D. Yao, "Determination of ku-band specific attenuation parameters based on measurements in the tropics," in *2013 IEEE Antennas and Propagation Society International Symposium (APSURSI)*, July 2013, pp. 2008–2009.

[25] P. Sharma, "Two year rain attenuation statistics over a line of sight terrestrial microwave link operating at 30 ghz in tropical region amritsar (india)," in *2011 XXXth URSI General Assembly and Scientific Symposium*, Aug 2011, pp. 1–4.

[26] T. Kozu, J. Awaka, H. Fukuchi, and K. Nakamura, "Rain attenuation ratios on 30/20- and 14/12-ghz satellite-to-earth paths," *Radio Science*, vol. 23, no. 03, pp. 409–418, May 1988.

[27] Y. Xiao, Z. Jinfeng, F. Jun, and L. Weimin, "Research on the ku band rain attenuation estimation algorithm," in *2015 IEEE International Conference on Computational Intelligence Communication Technology*, Feb 2015, pp. 583–586.

[28] W. Stutzman and W. Dishman, "A simple model for the estimation of rain-induced attenuation along earth-space paths at millimeter wavelengths," *Radio Science*, vol. 17, no. 06, pp. 1465–1476, 1982.

[29] L. J. Ippolito, "Radio propagation for space communications systems," *Proceedings of the IEEE*, vol. 69, no. 6, pp. 697–727, June 1981.

[30] M. Leitao and P. Watson, "Method for prediction of attenuation on earth-space links based on radar measurements of the physical structure of rainfall," in *IEE Proceedings F (Communications, Radar and Signal Processing)*, vol. 133, no. 4. IET, 1986, pp. 429–440.

[31] A. D. Panagopoulos, P.-D. M. Arapoglou, and P. G. Cottis, "Satellite communications at ku, ka, and v bands: Propagation impairments and mitigation techniques," *IEEE Communications Surveys & Tutorials*, vol. 6, no. 3.

[32] A. D. Panagopoulos, P.-D. Arapoglou, J. D. Kanellopoulos, and P. G. Cottis, "Long-term rain attenuation probability and site diversity gain prediction formulas," *IEEE Transactions on Antennas and Propagation*, vol. 53, no. 7, pp. 2307–2313, 2005.

[33] M. Bevis, S. Businger, T. A. Herring, C. Rocken, R. A. Anthes, and R. H. Ware, "Gps meteorology: Remote sensing of atmospheric water vapor using the global positioning system," *Journal of Geophysical Research: Atmospheres*, vol. 97, no. D14, pp. 15 787–15 801, 1992.

[34] A. Gharanjik, B. S. MR, P.-D. Arapoglou, and B. Ottersten, "Multiple gateway transmit diversity in Q/V band feeder links," *IEEE Transactions on Communications*, vol. 63, no. 3, pp. 916–926, 2015.

[35] B. Frénay and M. Verleysen, "Classification in the presence of label noise: a survey," *IEEE transactions on neural networks and learning systems*, vol. 25, no. 5, pp. 845–869, 2014.

[36] M. Schleiss and A. Berne, "Identification of dry and rainy periods using telecommunication microwave links," *IEEE Geoscience and Remote Sensing Letters*, vol. 7, no. 3, pp. 611–615, 2010.

[37] S. Haykin, *Neural Networks and Learning Machines*, ser. Neural networks and learning machines. Prentice Hall, 2009, no. v. 10.

[38] J. Heaton, *Introduction to neural networks with Java*. Heaton Research, Inc., 2008.

[39] M. H. Beale, M. T. Hagan, and H. B. Demuth, *Neural Network Toolbox Reference*. The MathWorks Inc., 2017.

[40] "ITU-R Recommendation P.838-3," *Specific attenuation model for rain for use in prediction methods*, 2005.

[41] "ITU-R Recommendation P.618-11," *Propagation data and prediction method required for the design of the Earth-space telecommunication systems*, 2013.

[42] "ITU-R Recommendation P.839-4," *Rain height model for prediction methods*, 2013.

[43] M. Kaufmann and J. Rieckermann, "Identification of dry and rainy periods using telecommunication microwave links," in *12nd International Conference on Urban Drainage, Porto Alegre/Brazil*, 2011, pp. 10–15.

[44] M. Schleiss, J. Rieckermann, and A. Berne, "Quantification and modeling of wet-antenna attenuation for commercial microwave links," *IEEE Geoscience and Remote Sensing Letters*, vol. 10, no. 5, pp. 1195–1199, 2013.

Ahmad Gharanjik received a M.S. Degree in Telecommunication Systems form K. N. Toosi University of Technology, Tehran, Iran in 2010. He was with Huawei Technology, Tehran from 2010 to 2012 as a WiMAX Performance Optimization Engineer. He received docteur en informatique degree from University of Luxembourg, Luxembourg and Ph.D. in electrical engineering from KTH Royal Institute of Technology, Stockholm, Sweden both in May 2016. He was a research associate at University of Luxembourg, SnT from June 2016 to September 2017. He is founder and CEO of Databourg Systems S.a r.l.-S. His current research interests include signal processing for satellite communication, machine learning and optimization.

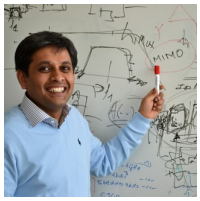

Bhavani Shankar M R (M'11) received Masters and Ph. D in Electrical Communication Engineering from Indian Institute of Science, Bangalore in 2000 and 2007, respectively. He was a Post Doc at the ACCESS Linnaeus Centre, Signal Processing Lab, Royal Institute of Technology (KTH), Sweden from 2007 to September 2009 and is currently a Research Scientist at SnT. He was with Beceem Communications, Bangalore from 2006 to 2007 as a Staff Design Engineer working on Physical Layer algorithms for WiMAX compliant chipsets. He was a visiting student at the Communication Theory Group, ETH Zurich, headed by Prof. Helmut Bölcskei during 2004. Prior to joining Ph. D, he worked on Audio Coding algorithms in Sasken Communications, Bangalore as a Design Engineer from 2000 to 2001. He is currently on the executive committee of the IEEE Benelux joint chapter on communications and vehicular technology and serves as the Handling Editor for Elsevier Signal Processing. Since 2018, he is also on EURASIP Special Area Team on Theoretical and Methodological Trends in Signal Processing (SAT-TMTSP). He was a co-recipient of the IEEE Communications Society Satellite and Space Communications Technical Committee (SSC-TC) award for Distinguished Contributions to Satellite Communications in 2014. His research interests include statistical signal processing, wireless communications, resource allocation, game theory and fast algorithms for structured matrices.

Frank Zimmer received the Diploma Ing. (FH) degree in electrical engineering from the University of Applied Sciences in Kaiserslautern (Germany) and the DEA Diploma in signal theory and communications from the University of Vigo (Spain). He is a Senior Manager at SES Networks where he heads the systems engineering section. His research interests include autonomous agents and multi-agent systems, embedded systems, software radio technologies and systems engineering. He is a member of IEEE, IEEE Computer Society, ACM and INCOSE. Contact him at frank.zimmer@ses.com.

Björn Ottersten (S'87-M'89-SM'99-F'04) was born in Stockholm, Sweden, 1961. He received the M.S. degree in electrical engineering and applied physics from Linköping University, Linköping, Sweden, in 1986. In 1989 he received the Ph.D. degree in electrical engineering from Stanford University, Stanford, CA.

Dr. Ottersten has held research positions at the Department of Electrical Engineering, Linkping University, the Information Systems Laboratory, Stanford University, the Katholieke Universiteit Leuven, Leuven, and the University of Luxembourg. During 96/97 Dr. Ottersten was Director of Research at ArrayComm Inc, a start-up in San Jose, California based on Ottersten's patented technology. He has co-authored journal papers that received the IEEE Signal Processing Society Best Paper Award in 1993, 2001, 2006, and 2013 and 7 IEEE conference papers receiving Best Paper Awards. In 1991 he was appointed Professor of Signal Processing at the Royal Institute of Technology (KTH), Stockholm. From 1992 to 2004 he was head of the department for Signals, Sensors, and Systems at KTH and from 2004 to 2008 he was Dean of the School of Electrical Engineering at KTH. Currently, Dr. Ottersten is Director for the Interdisciplinary Center for Security, Reliability and Trust at the University of Luxembourg. Dr. Ottersten is a board member of the Swedish Research Council and a Digital Champion of Luxembourg, he acts as advisor to the European Commission.

Dr. Ottersten has served as Associate Editor for the IEEE Transactions on Signal Processing and on the editorial board of IEEE Signal Processing Magazine. He is currently editor of EURASIP Signal Processing Journal and a member of the editorial boards of EURASIP Journal of Applied Signal Processing and Foundations and Trends in Signal Processing. Dr. Ottersten is a Fellow of the IEEE and EURASIP and a member of the IEEE Signal Processing Society Board of Governors. In 2011 he received the IEEE Signal Processing Society Technical Achievement Award. He has received the European Research Council's advanced research grant twice, 2009-2013 and 2017-2021.

His research interests include security and trust, reliable wireless communications, and statistical signal processing. Ottersten is a Fellow of the IEEE and EURASIP and a member of the IEEE Signal Processing Society Board of Governors. In 2011 he received the IEEE Signal Processing Society Technical Achievement Award. He has received the European Research Council's advanced research grant twice, 2009-2013 and 2017-2021.